ChemSusChem

Research Article
doi.org/10.1002/cssc.202300137

Chemistry Europe
European Chemical Societies Publishing

www.chemsuschem.org

Divide and Conquer: A Novel Dual-Layered Hydrogel for Atmospheric Moisture Harvesting

An Feng,[a] Casey Onggowarsito,[a] Shudi Mao,[a] Greg G. Qiao,[b] and Qiang Fu*[a]

Atmospheric water harvesting (AWH) has been recognized as a next-generation technology to alleviate water shortages in arid areas. However, the current AWH materials suffer from insufficient water adsorption capacity and high-water retention, which hinder the practical application of AWH materials. In this study, we developed a novel dual-layered hydrogel (DLH) composed of a light-to-heat conversion layer (LHL) containing novel polydopamine-manganese nanoparticles (PDA–Mn NPs) and a water adsorption layer (WAL) made of 2-(acryloyloxyethyl) trimethylammonium chloride (AEtMA). The WAL has a strong ability to adsorb water molecules in the air and has a high-water storage capacity, and the PDA–Mn NPs embedded in the LHL have excellent photothermal conversion efficiency, leading to light-induced autonomous water release. As a result, the DLH displays a high-water adsorption capacity of 7.73 $g\,g^{-1}$ under optimal conditions and could near-quantitatively release captured water within 4 h sunlight exposure. Coupled with its low cost, we believed that the DLH will be one of the promising AWH materials for practical applications.

Introduction

Freshwater has been one of the most essential parts of human life since the origination of human beings. On earth, there are 1.46×10^{16} tons of water exist, where less than 0.03% (various surface freshwater) can be currently used by human being.[1] Of the surface freshwater, ca. 3% (1.31×10^{11} tons) is stored in the atmosphere, however there are limited methods to effectively collect this freshwater.[2,3] Water in the atmosphere exists in two forms: water vapor (unsaturated water in the form of molecules) and fog or cloud (saturated water in the form of small droplets). People have a long history of producing freshwater through proactive dew water harvesting methods that use chemical coolants and/or consume electricity (ca. 0.75 kWh per kilogram of liquid water).[4] But this energy-intensive method is not suitable for rural areas.

Inspired from desiccant and dehumidifier, scientists have recently developed water harvesting materials,[4,5] such as hygroscopic chemicals, metal oxides, metal–organic frameworks (MOFs), hydrogels, and composite materials composed of two or more of the aforementioned materials. These AWH materials are capable of adsorbing unsaturated atmospheric water at night when the temperature is low and the relative humidity (R.H.) is high and then releasing liquid water during the daytime. For instance, hygroscopic chemicals (e.g., calcium chloride, lithium chloride) are considered potential materials due to their high polarity and the ability to form hydrate with water molecules.[6] However, the released water could be contaminated if the halogen or hydroxide ions are leached.[7,8] As an alternative solution, customized hydrogels have proven to have greater water adsorption capacity, high swelling ratio and easier/faster water release compared with other AWH materials. However, it has been noted that for hydrogel systems, there are often trade-offs between water adsorption capacity and water release efficiency, and/or photothermal conversion efficiency and mechanical properties. For example, introducing metal–organic frameworks (MOFs) into poly(*N*-isopropylacrylamide) (PNIPAM) hydrogel leads to an improved capture capacity of 3 $g\,g^{-1}$ within 12 h compared to the bare counterparts due to the highly porous structure of MOFs for water storage.[9] However, the captured water is trapped in the pores of MOFs, resulting in a high proportion of retention water. Yu et al. reported a PNIPAM hydrogel that incorporated chloride-doped polypyrrole (PPy–Cl) as photo-thermal material (PTM) and auxiliary adsorbent. This hydrogel surprisingly achieved a water adsorption capacity of 6.2 $g\,g^{-1}$, and 50% of the captured water in the hydrogel can be self-released within 20 min under sunlight irradiation.[10] However, the delocalization of H^+ and Cl^- leads to response attenuation of PNIPAM hydrogel, resulting in an increasingly slower rate of water release. In another case, lithium chloride and reduced graphene oxide (rGO) were mixed with polyvinyl alcohol (PVA) and the resultant hydrogel showed a water adsorption capacity of 2.25 $g\,g^{-1}$. The incorporation of rGO improved the mechanical property of the hydrogel as the expense of water adsorption capacity.[11–13] We thus saw this as an opportunity to develop a novel dual-layered hydrogel (DLH) system with independent

[a] *A. Feng, C. Onggowarsito, S. Mao, Dr. Q. Fu*
Centre for Technology in Water and Wastewater, School of Civil and Environmental Engineering
University of Technology Sydney
NSW 2007, Australia
E-mail: Qiang.fu@uts.edu.au
[b] *Prof. G. G. Qiao*
Polymer Science Group, Department of Chemical Engineering
University of Melbourne Parkville
Melbourne, Victoria 3010 Australia

Supporting information for this article is available on the WWW under https://doi.org/10.1002/cssc.202300137

functions, one layer for water adsorption and storage, and the other for efficient, sunlight-assisted water release, to address the trade-offs.

In this work, we adopted a novel design strategy to prepare a DLH consisting of a light-to-heat conversion layer (LHL) and a water adsorption layer (WAL) to achieve stimuli-responsive water release and improved adsorption capacity simultaneously. The LHL was prepared by incorporating novel polydopamine-manganese(II) nanoparticles (PDA–Mn NPs) into PNIPAM matrix, and the WAL was prepared by copolymerizing NIPAM (< 25 wt%) and 2-(acryloyloxyethyl) trimethylammonium chloride (AEtMA, 75 wt%). In humid environment, the resultant DLH can effectively adsorb the moisture in the air and achieve a high-water adsorption capacity of 7.73 $g\,g^{-1}$. Of note, at low temperature the LHL layer can also absorb and store water in the PNIPAN matrix as well as the pores of PDA–Mn NPs. Under sunlight exposure, 50% of captured water was released within 1 h, and almost 100% adsorbed water can be released within 4 h.

Results and Discussion

To improve the water adsorption of hydrogel-based AWH materials while achieving stimulus release of water, we adopt the 'divide and conquer' strategy to prepare a novel functionally independent DLH. We first considered the use of dopamine-iron(III) (PDA–Fe) NP as PTM to construct light-to-heat conversion layer (LHL) because it is cheap and easy to synthesize. However, recent study has shown that Mn^{VII} ions can accelerate the redox cycle of dopamine by an order of magnitude compared Fe, Cu, Zn, and Co at micromolar concentrations.[14] We were curious whether the high degree of polymerization of polydopamine could lead to different photothermal properties. In this study, we synthesized a novel PDA–Mn NP and compared its photo-thermal conversion performance with that of PDA–Fe NP (Figure 1A).[15] It is found that the prepared PDA–Mn NPs have a diameter of 150–200 nm (Figure 1B and Figure S1 in Supporting Information) and can be homogeneously dispersed in aqueous media. While at low pH < 4, the PDA–Mn NPs tend to form aggregations. We further conducted energy dispersive X-ray (EDX) analysis of the PDA–Mn NPs (Figure 1C). Except C, N and O elements, we observed two characteristic peaks belonging to manganese at 655 and 790 eV. In contrast, the PDA–Fe NPs have a larger diameter of 500 nm (Figure S1).

We then prepared a series of LHLs consisting of poly(*N*-isopropylacrylamide) (PNIPAM) matrix and PDA–Mn NPs PTM (or PDA–Fe NPs as a control sample) via radical polymerization at room temperature according to previous report[10]

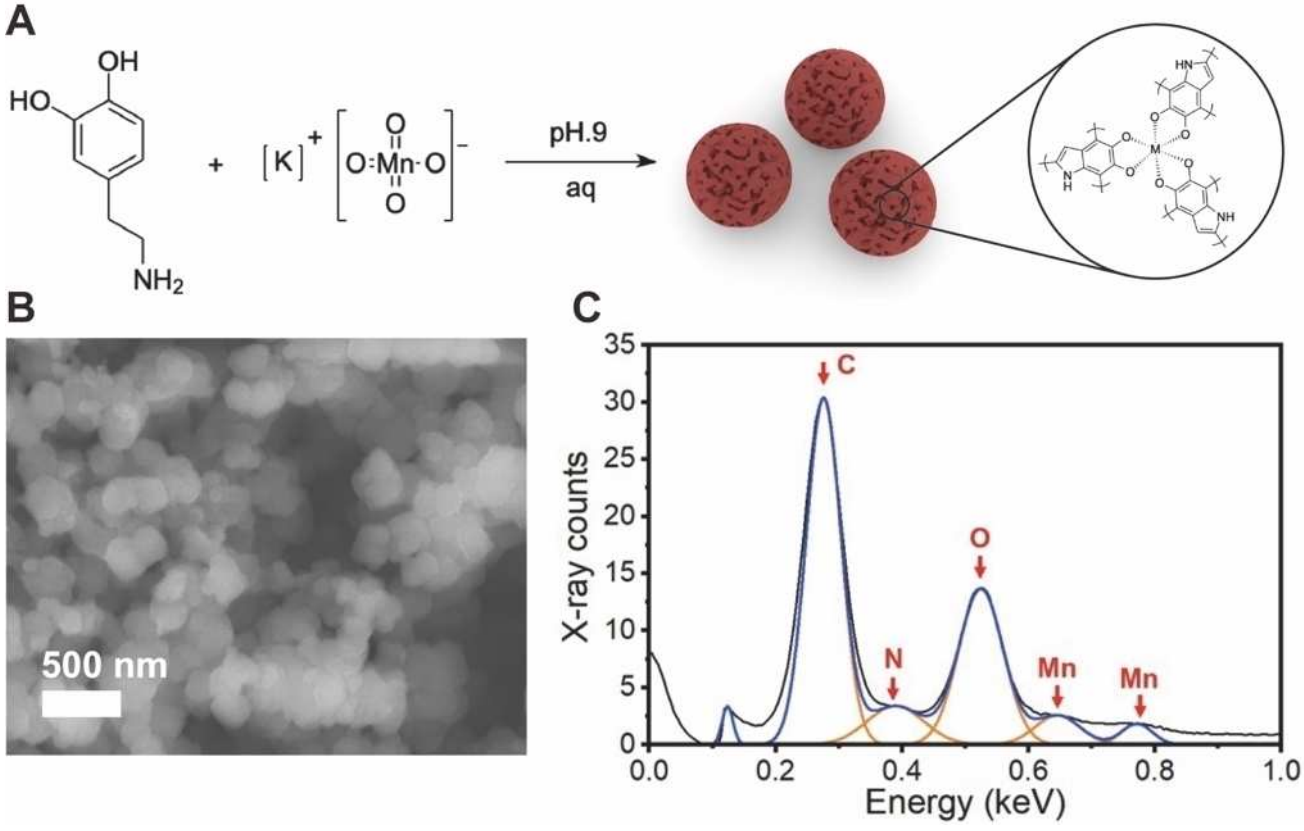

Figure 1. A) The synthesis of polydopamine-(Mn) nanoparticles (PDA–Mn NPs). B) SEM images of PDA–Mn NPs. C) Energy dispersive x-ray (EDX) analysis result for element identification using multiple peaks fitting (Black: original EDX data; Blue: accumulative curve from fitted peaks; Orange: carbon, nitrogen, oxygen, and manganese peak).

(Scheme 1). As expected, the resultant LHLs containing 5–10 wt% NPs displayed stronger solar absorption ability compared to the bare sample (0 wt%) in all UV-VIS-NIR ranges (250–2000 nm, Figure 2A). Of note, further increasing the loading of

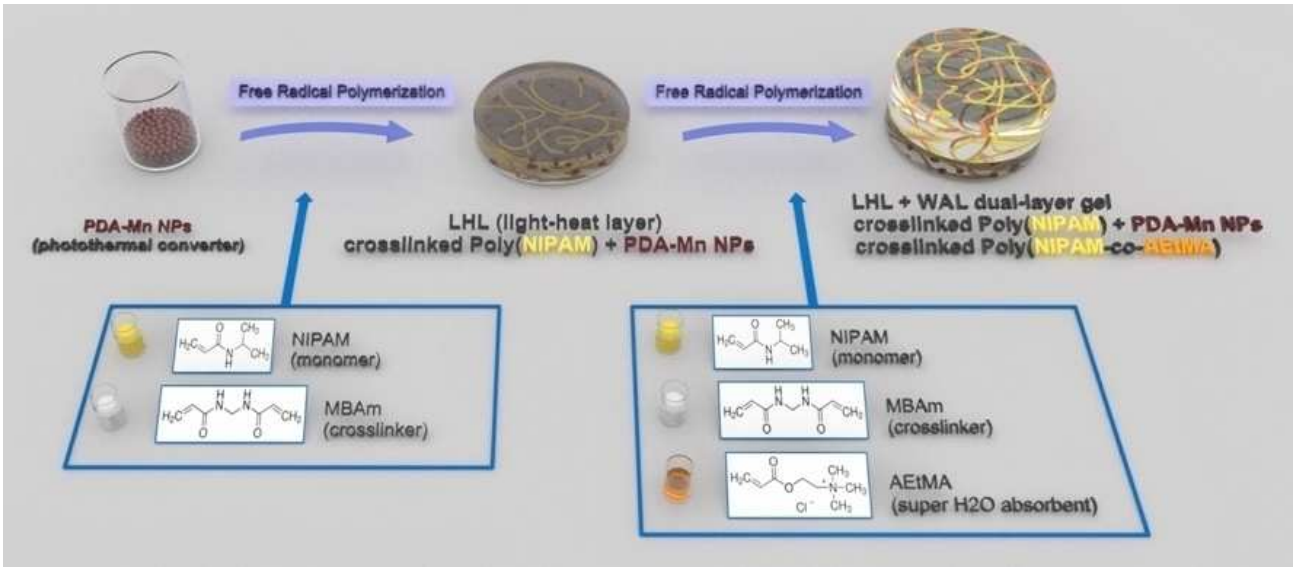

Scheme 1. Schematic illustration of the synthesis of dual-layered composite hydrogel.

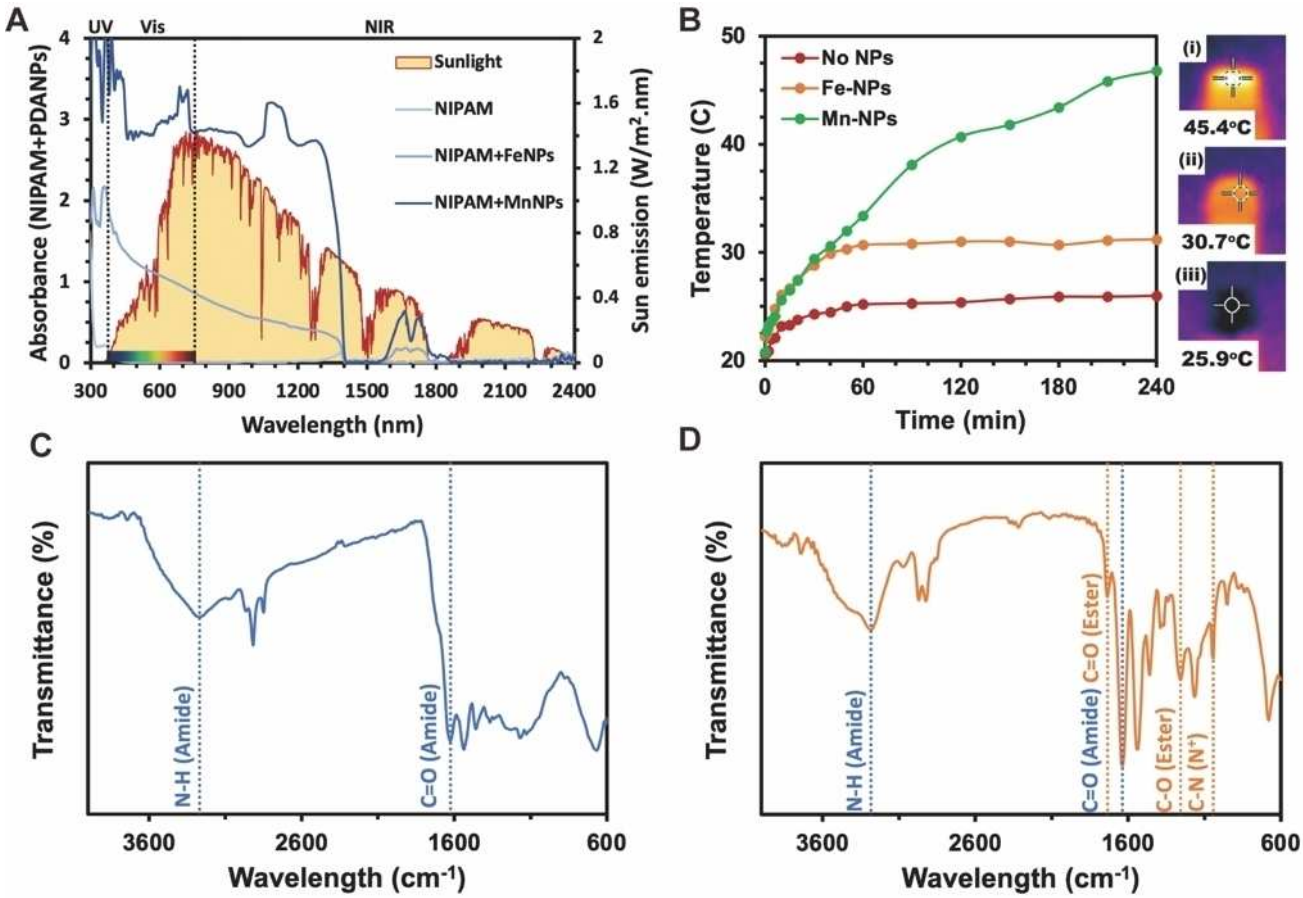

Figure 2. A) Absorption spectra of LHLs vs. sunlight emission spectrum. B) Temperature profiles of the prepared LHLs ($1\times1\times1$ cm^3) under 1.0 sun irradiation for 4 h without NPs (red), with PDA–Fe NPs (orange) or with PDA–Mn NPs (green). C) FTIR spectrum of PNIPAM-based LHL. D) FTIR spectrum of PNIPAM/PAEtMA-based WAL.

PDA–Mn NPs leads to aggregation of NPs, and the resulting LHL showed incremental photothermal response. We then evaluated their photothermal converting ability. As shown in Figure 2B, the bare sample without NPs showed a consistent temperature of 25 °C after 1 h of sunlight irradiation (1.0 sun equivalent). The LHL containing PDA–Fe NPs reached ca. 30 °C after 1 h irradiation and maintained this temperature. This may be attributed to the severe aggregation of PDA–Fe NPs in PNIPAM matrix, resulting in low conversion efficiency. In contrast, the temperature of the LHL with PDA–Mn NPs increased from room temperature to 33 °C within 1 h and continued to rise to 45.4 °C in the next 3 h. These results indicate that the uniformly dispersed PDA–Mn NPs are more effective in the absorption and conversion of sunlight into heat. The structure of PNIPAM-based LHL was further characterized by FTIR spectroscopy (Figure 2C). We observed the characteristic peaks at 1650 and 3300 cm^{-1}, which can be attributed to the C=O stretching and N–H stretching of PNIPAM, respectively.

Previous study has demonstrated that the PNIPAM-based, monolayer hydrogel system usually has an insufficient moisture adsorption capacity at unsaturated environment.[10] To address this issue, we further synthesized a polyelectrolyte-based water adsorption layer (WAL) to enhance water capture and storage. Polyelectrolytes are polymers possessing ionizable groups[16] and have been widely used in the treatments of wastewater, ceramic slurries, and concrete mixtures.[17–21] Due to their super-hydrophilic ionizable groups, polyelectrolyte-based hydrogels show an unusual high swelling ratio of $>100\ g\,g^{-1}$.[22] In this study, an aqueous mixture containing monomers, [NIPAM]/[AEtMA] = 1:3, where NIPAM = *N*-isopropylacrylamide and AEtMA = 2-(acryloyloxyethyl) trimethylammonium chloride, and crosslinker was poured on the prepared LHL, and the WAL was prepared via radical copolymerization (Scheme 1). The resulting DLHs were then frozen at −20 °C and thawed in DI water to remove unreacted residue, followed by frozen-drying. The WAL is composed of 75 wt% poly([2-(acryloyloxy)ethyl] trimethylammonium chloride), PAEtMA, leading to an exceptional affinity for water molecules due to the strong polarity of quaternary ammonium-chloride groups of AEtMA. While the remaining ca. 25 wt% PNIPAM component can enhance the compatibility between WAL and LHL. To demonstrate the high-water affinity of the WAL, we prepared a control sample with the same composition (i.e., AEtMA/NIPAM = 3:1 *wt*/*wt*) and evaluated its water uptake capacity. As expected, this sample had a maximum water uptake capacity of 131.75 g of water per gram of dry gel (Figure S2 in Supporting Information). This result is much higher than that of the PNIPAM-based hydrogels.[10]

The surface (both the LHL and the WAL surfaces) and the cross-sectional morphologies the DLH were measured by SEM images (Figure 3A–F). The SEM images (Figure 3A,B,D,E) confirm that both layers have a highly porous structure and hence high surface area. In addition, the PNIPAM/PAEtMA-based WAL has a 'thicker wall' and larger pore size in comparison with the PNIPAM/NPs-based LHL. This result may be attributed to the lower glass transition temperature (*Tg*) of PAEtMA, resulting in a 'slower' solidification process in the freezing dry.[23] We also observed a clear boundary between the two layers (Figure 3C) and the connection is stable without sign of detachment. This result proves the successful preparation of the DLH, a rarely reported AWH material. When we zoomed in to the SEM image of LHL, we clearly observed the PDA–Mn NPs embedded into the PNIPAM 'wall' (Figure 3F). This is in good agreement with the EDX mapping result (Figure S3 in Supporting Information). The vertical pores on hydrogel surface provides adequate adsorption area for water molecules as well as transport channels for liquid water. Moreover, the highly porous structure of LHL will also facilitate the fast water release via evaporation.

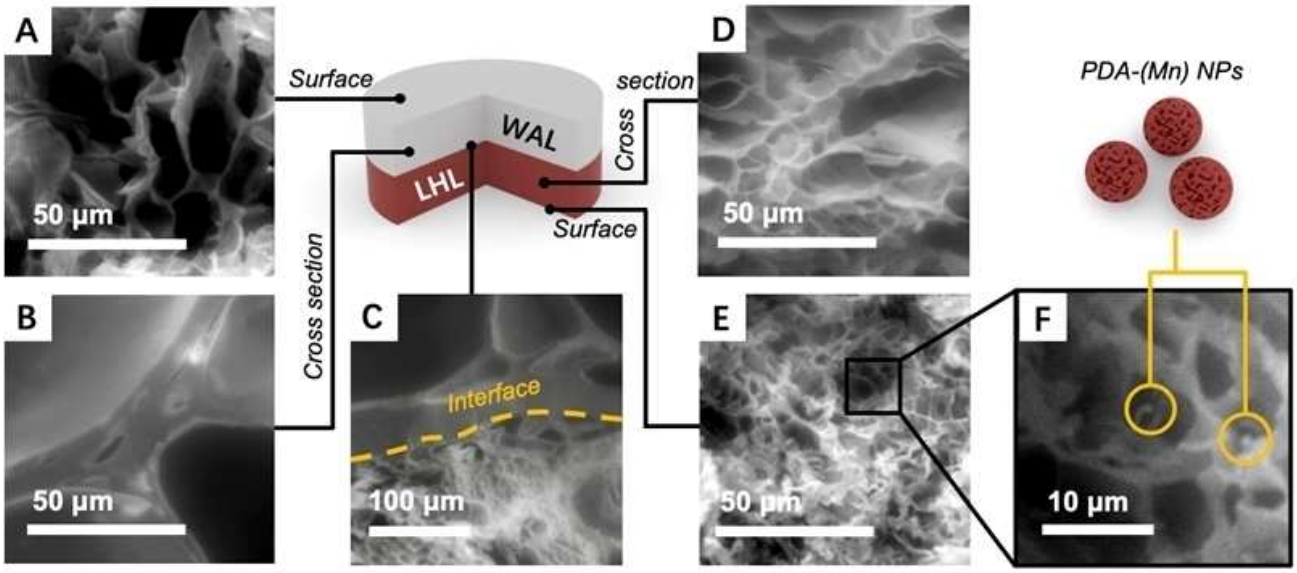

Figure 3. SEM images of the dry dual-layered hydrogel: A) WAL surface, B) WAL cross-section, C) interface between WAL and LHL, D) LHL cross-section, E) LHL surface, and F) enlarged section of (F) indicating the PDA–Mn NPs.

The structure of PNIPAM/PAEtMA-based WAL is also characterized by FTIR spectroscopy (Figure 2D). Two new peaks at 1250 and 1700 cm^{-1} were observed, which can be attributed to the vibration of C–O and C=O of PAEtMA, respectively. The apparent peak at 1,000 cm^{-1} indicates the presence of quaternary ammonium groups,[24] that have strong electrostatic forces with water molecules in the atmosphere.

To validate the concept of 'divide and conquer' strategy, we first compared the water capture and release performance of the DLHs with a monolayer counterpart which contains the same compositions. The control sample was prepared by simply mixing the same amount of NIPAM, AEtMA, crosslinker and PDA–Mn NPs, followed by copolymerization and freeze-thaw under the same conditions. Both the DLH and the control sample were placed in a sealed plastic container to prevent condensed water contact. The container was cooled down and a moisture airflow with constant relative humidity (R.H. was supplied by passing compressed dry air through saturated salt solutions.[10] The DLH adsorbed water up to ca. 2.5 $g\,g^{-1}$ at >90% R.H., which is ca. 60% higher than that of the control sample (Figure S4 in Supporting Information). This result can be attributed to the formation of random copolymers of NIPAM and AEtMA in the monolayer gel, disrupting the long-range continuity of more hydrophilic PAEtMA segments. Once the WAL was saturated, the water adsorbed can be transferred to the LHL by capillary force. In the LHL, the porous PDA–Mn NPs with a large number of phenolic hydroxyl groups offer high water affinity and additional storage space. The water adsorbed into the DLH can be released under sunlight irradiation by evaporation. Specifically, PDA–Mn NPs in LHL can convert electromagnetic waves into thermal energy to heat the hydrogel. In this study, the LHL can reach more than 45 °C under simulated sunlight exposure within 4 h, promoting rapid evaporation of water molecules stored in the DLH. In the following evaporation tests, we found that the evaporation rate of the control sample is 0.125 $g\,g^{-1}\,min^{-1}$, which is slightly higher than that of DLH (0.1 $g\,g^{-1}\,min^{-1}$). This result can be attributed to the higher heat conductivity of the monolayer gel. In short, these results indicate that besides the chemical composition, the hydrogel architecture also plays a key role in the water adsorption and release performance. In the plastic container, the surface of the hydrogel is close to 5 °C and the temperature of the inner wall is close to 0 °C. As shown in Scheme S1B, the temperature of the vapor in the container drops sharply on the surface of the hydrogel, thus crossing the dew point and condensing into water. The water vapor in the remaining space remains in the gas phase.

In the DLH, the WAL has a higher water adsorption capacity than the LHL, leading to a huge shear force at the interface, which may trigger layer detachment and even tear the WAL. We thus optimized the composition of DLH by tuning the mass loading of PDA–Mn NPs, the composition of WAL and the weight ratio of LHL and WAL. Figure 4A illustrates the moisture adsorption and water release performance of a series of DLHs containing 0, 5, 10, and 15 wt% PDA–Mn NPs in the LHL. Increasing mass loadings of PDA–Mn NPs brings an improved moisture capture capacity by ca. 80% during a continuous 12 h experiment. In the subsequent simulated evaporation/release process, the DLHs can release 50% of captured water within 1 h ($t_{0.5}$ = 1 h) under sunlight irradiation (1.0 sun equivalent). It is also found that 10 wt% of PDA–Mn NPs load is the optimal amount for LHL. Because further increasing PDA–Mn NPs loading to 15 wt% led to aggregation of NPs, and thus has a negligible effect on water evaporation rate.

During the moisture adsorption process, water molecules first collide with the WAL surface, and the density of the quaternary ammonium salt determines its water affinity. Therefore, we optimized the moisture adsorption capacity of the DLH by judicious adjusting the composition of the WAL. We fixed the volume ratio of LHL/WAL = 1:1 and the PDA–Mn NPs content of 10 wt% in the LHL, and then prepared a series of DLHs with different NIPAM/AEtMA weight ratio of 4:0, 3:1, 2:2 and 1:3. Of particular note, further increasing AEtMA content to 100 wt% led to a poor compatibility towards PNIPAM-based LHL. Figure 4B illustrates the moisture capture and water release performance of these DLHs. Due to the strong water affinity of quaternary ammonium cations, the low moisture density close to the surface creates a humidity gradient that becomes the main driving force for moisture capture. Thus, with the increase of AEtMA content from 0 to 75 wt% (1:3), the moisture capture capacity of the resulting DLHs increased by 110%. Again, this result indicates that PAEtMA has a significantly larger moisture-adsorbing ability compared with PNIPAM. Interestingly, all the prepared DLHs can release 50 wt% captured water within 1 h under sunlight exposure, suggesting efficient water transport from WAL to LHL. This is also proved in the stable gradient region detailed in Supporting Information (Figure S5).

Despite the high moisture capture capacity of the WAL with 75 wt% of AEtMA, we further optimized the volume ratio of WAL to LHL to boost the overall water adsorption capacity, while maintaining the ability to rapidly release water. Four DLHs with different volume ratios of LHL to WAL (LHL/WAL = 3:1, 2:2, 1:2, and 1:3, *v*/*v*) were prepared. In the water capture experiment, we found that the moisture capture capacity increased from 2.41 to 7.73 $g\,g^{-1}$ when gradually increasing the WAL volume ratio (Figure 4C). Under sunlight exposure, all the DLHs showed a $t_{0.5}$ = 1 h and can release >98% of captured water in 4 h. Meanwhile, the top surface temperature of the LHL achieved 50 °C during water desorption, and the average of the DLH reached 42.5 °C (Figure S6 in Supporting Information). Under extreme conditions, such as when DLH is in direct contact with water, the LHL/WAL = 3:1 (*v*/*v*) DLH has a maximum water uptake of 18.51 $g\,g^{-1}$. While this value increases to 22.15 $g\,g^{-1}$ in the case of LHL/WAL = 1:3 (*v*/*v*).

At 5 °C, The water adsorption performance of DLH is also different under different relative humidity environments. The prepared DLH exhibited an excellent water adsorption capacity of 4.55 $g\,g^{-1}$ and 7.73 $g\,g^{-1}$ in 12 h under 90% and 95% R.H., respectively. While, under moderate (75% R.H.) or low (<60% R.H.) humidity conditions, the water adsorption capacity of DLH were 1.75 $g\,g^{-1}$ and 1.21 $g\,g^{-1}$, respectively (Figure 4D). The water adsorption capacity of the DLH increased by 341.7% from 60% to 95% R.H. This result can be attributed to the difference

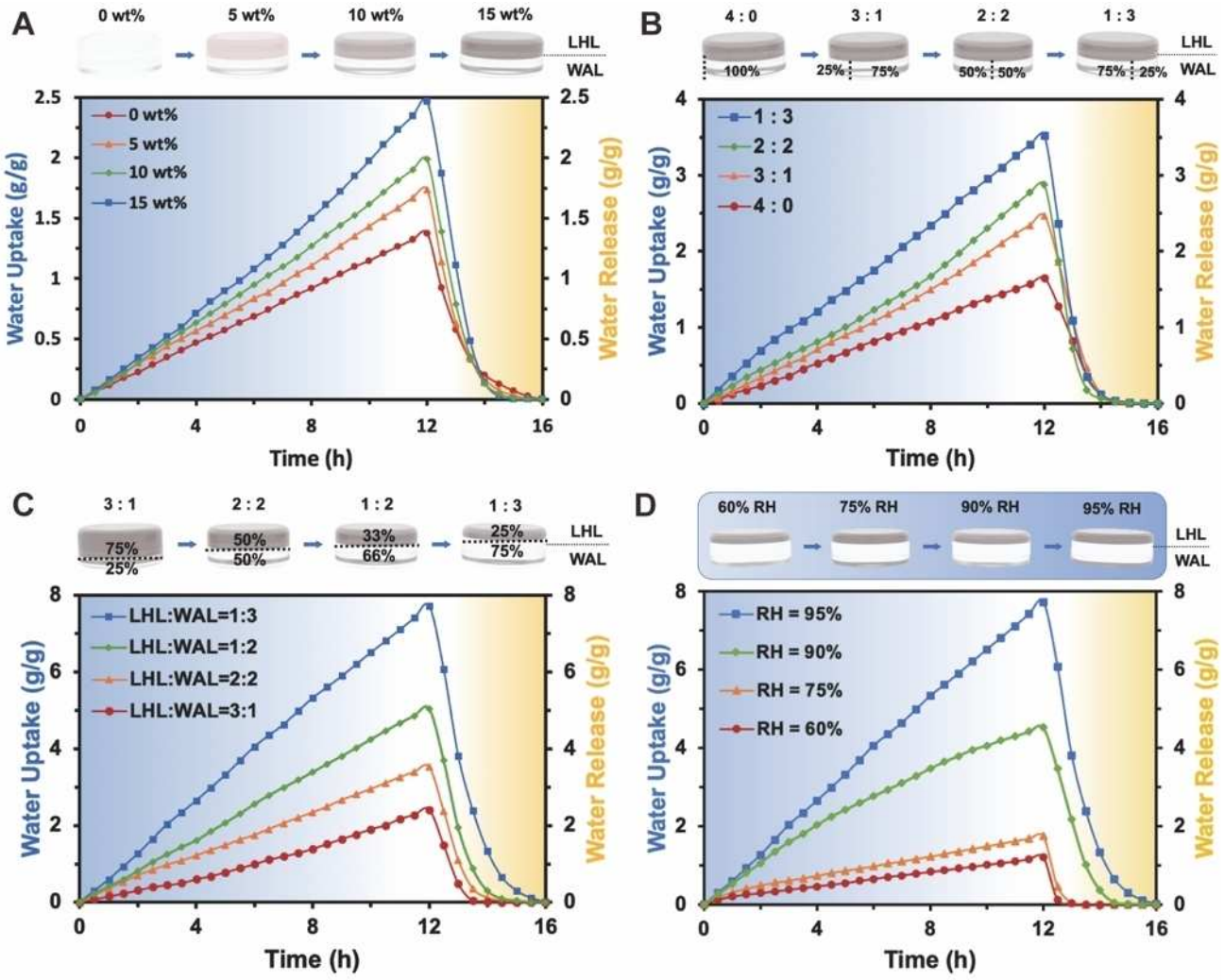

Figure 4. A) Indoor moisture capture simulation using dual-layered hydrogel with 0, 5, 10, and 15 wt% PDA–Mn NPs under 1.0 sun irradiation (LHL/WAL = 1:1). B) Indoor moisture capture simulation using dual-layered hydrogel with 4:0, 3:1, 2:2, and 1:3 mass ratio between NIPAM and AEtMA at 95% RH and 5 °C. C) Indoor moisture capture simulation using dual-layered hydrogel with 1:3, 1:2, 2:2, and 3:1 *v/v* between LHL and WAL at 95% RH and 5 °C. D) Indoor moisture capture simulation using dual-layered hydrogel with 1:3 *v/v* between LHL and WAL at 60%, 75%, 90%, and 95% RH at 5 °C.

in water vapor density under moderate (0.0033-gram water vapor per gram of dry air) and high humidity (0.0052 $g\,g^{-1}$), resulting in insufficient water molecules to achieve passive dewing under moderate or low humidity conditions. We found that upon continuing to increase the humidity to >100% R.H. (i.e., fog), the water absorption capacity of DLH was *ca.* 18.1 $g\,g^{-1}$ within 12 h and showed a tendency to reach equilibrium (Figure S7A). However, this value is still lower than the maximum swelling ratio of the DLH.

While when the temperature gradually increased from 5 °C to 25 °C, the water adsorption capacity of DLH decreased from 7.73 $g\,g^{-1}$ to 1.24 $g\,g^{-1}$ (Figure S7B). As the temperature increases, the time required for vapor to liquefy on the surface of the DLH increases. The change in adsorption mechanism was reflected in the fact that the water adsorption curve tended to approach the plateau stage, that is, gradually reached equilibrium at higher temperatures.

We further tested the static water adsorption capacity of DLH at 25 °C, 15 °C and 5 °C respectively and compared the results with the dynamic water adsorption capacity under the same conditions. As shown in Figure S8A, at 25 °C the difference between the dynamic and static water adsorption capacity of DLH was the smallest, only 14.6%. The largest difference in water adsorption capacity (>97%) was observed as the temperature decreased to 5 °C (Figure S8C). This is because as the temperature decreases, the absolute humidity of water vapor decreases rapidly in air with the same relative humidity. This leads to a sharp decrease in the density difference of water molecules (or vapor concentration difference) near the surface of the DLH, with a corresponding decrease in the driving force for liquefaction.

Due to its highly porous structure and numerous open metal sites, metal–organic frameworks (MOFs) have been incorporated into hydrogel-based AWH materials to improve water storage capacity.[25–31] However, such hydrogels usually

displayed a relatively low water release efficiency because water molecules stored in the porous MOF NPs lack the driving force to efflux.[32,33] In contrast, we found that the water release efficiency of the DLH containing porous PDA–Mn NPs reached 98.4%, which is much higher than MOF-based AWH materials. In this study, the PDA–Mn NPs can generate heat in situ and the electrostatic attraction between the open metal sites and water molecules was then suppressed at elevated temperature, thus giving the water molecules greater kinetic energy and weakening the hydrogen bonding with PDA–Mn NPs.[34–37] In addition, the water adsorption capacity can also positively affect the evaporation rate. As shown in Figure S5, corresponding to the LHL/WAL = 3:1, 1:1, 1:2, and 1:3 (*v*/*v*) DLHs, the water evaporation rates were 0.09, 0.12, 0.1, and 0.09 $g\,g^{-1}\,min^{-1}$, respectively. Nevertheless, the advantage of thickening WAL is still extremely outweighing the disadvantage of thinning the LHL.

We then compared the moisture capture capacity and water releasing efficiency of the present DLH with the state-of-the-art AWH materials. As shown in Figure 5, the vast majority of AWH materials are hydrogel- and MOF-based systems. For hydrogel materials, under the optimized adsorption conditions (i.e., 80–95% R.H.), they typically exhibit high water release efficiencies, >85%, but have diverse water adsorption capacities (Figure 5). In the case of MOFs, they work under relatively low humidity conditions (<80% R.H.) and exhibit lower adsorption capacity and lower release efficiency. Compared with these AWH materials, the present DLH exhibits the highest water adsorption capacity of 7.73 $g\,g^{-1}$ at 95% R.H. and a very high-water release efficiency of 96.7% with a moderate water release rate of $t_{0.5}$ = 59 min under sunlight exposure. Under the condition of 75–90% R.H., the comprehensive performance of the present DLH is still in the top tier. At ≤60% R.H., the DLH still shows competitive water capture capacity and higher release efficiency compared to MOF-based AWH systems. This performance is also higher than all hydrogel-based AWH materials. Notably, the DLH exhibits a 60% increase in water adsorption capacity compared to the monolayer hybrid hydrogel with the same composition (the control sample) (Figure S4 in Supporting Information). These results suggest that the current mainstream hybrid AWH hydrogels have enormous potential to further improve the water adsorption efficiency after functional separation using this "divide and conquer" strategy.

To ensure that the DLH can withstand multiple water adsorption and release cycles, we then performed a cyclic durability test (Figure 6A). Each cycle includes 8 h water adsorption under 95% R.H. and 4 h water release under sunlight irradiation. After each releasing process, the hydrogels were exposed to sunlight for an additional 1 h to remove any residual water. After 10 cycles, the DLH (LHL/WAL = 1:3, *v*/*v*) displayed an average water adsorption capacity of 5.31 $g\,g^{-1}$, with an error of <5%. After 4 h of sunlight exposure, the average water release efficiency was ca. 97%. Under sunlight exposure, the LHL can convert electromagnetic waves into heat and undergo axial shrinkage due to the thermal response of PNIPAM. This deform provides the WAL with a horizontal shear force towards the axis, which physically promotes the rapid evaporation of liquid water inside the WAL (Figure 6B). Thereafter, we again performed SEM characterization of the DLH sample to investigate its interface morphologies. As shown in Figure S9 (Supporting Information), no layer detachment was observed after 10 cycles. This result thus demonstrates that the introduction of NIPAM (25 wt%) component into the WAL can enhance its compatibility with LHL.

To further investigate the practical water adsorption and desorption performance, a laboratory-made water harvesting device was built as shown in Figure 7A. This device consists of a rectangular container and a rectangular cap with sloping top

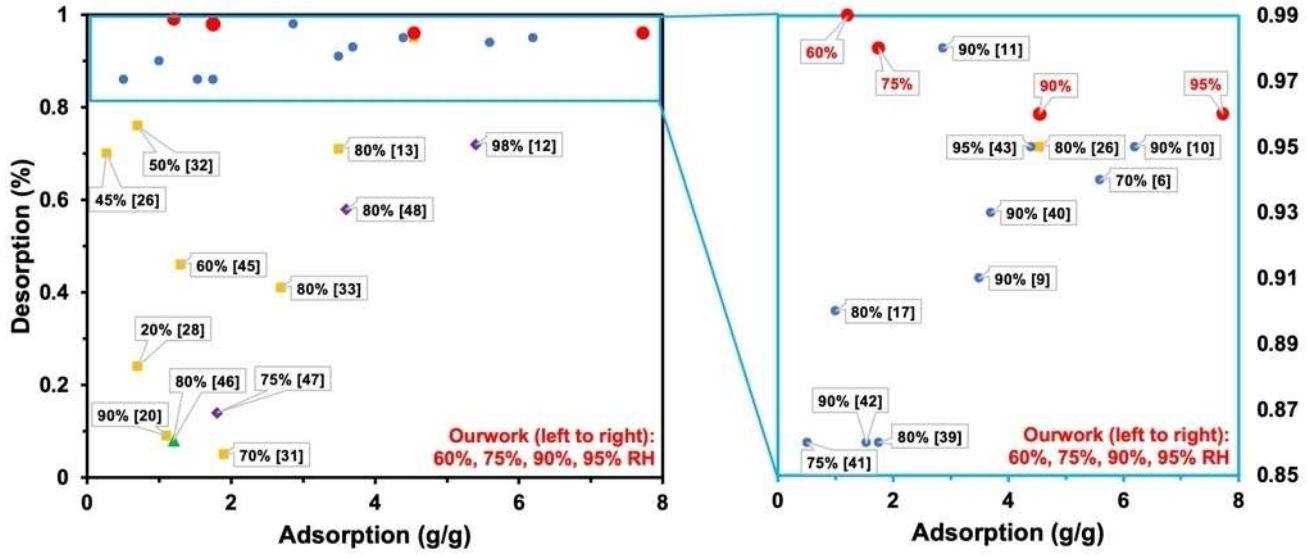

Figure 5. Recent publications of sorption based AWH materials and their unsaturated water adsorption and release efficiency. Comments of each dot refers to the value of experimental relative humidity and reference. (Blue dots: hydrogel;[6,9,10,16,38–42] Yellow rectangle: MOF;[13,25,27,30–33,43,44] Green triangle: ionic liquid;[45] Purple diamond: hygroscopic inorganic compounds;[12,46,47] Red dots from left to right: our work at 75%, 90%, and 95% RH conditions).

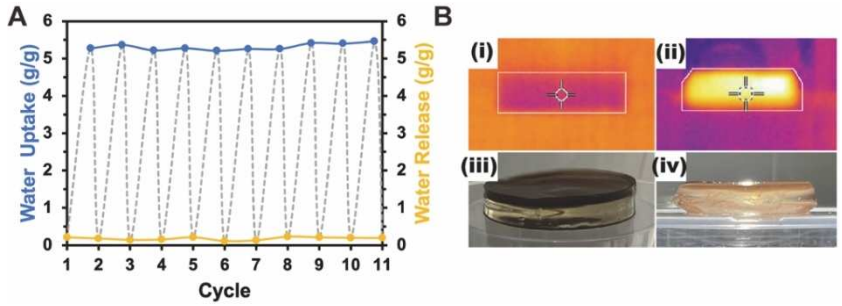

Figure 6. A) Durability performance of dual-layered hydrogel with LHL/WAL = 1 : 3 (volume ratio). B) Temperature measurement and the appearance of dual-layered hydrogel under simulated sunlight irradiation (1.0 sun equivalent) for 30 min.

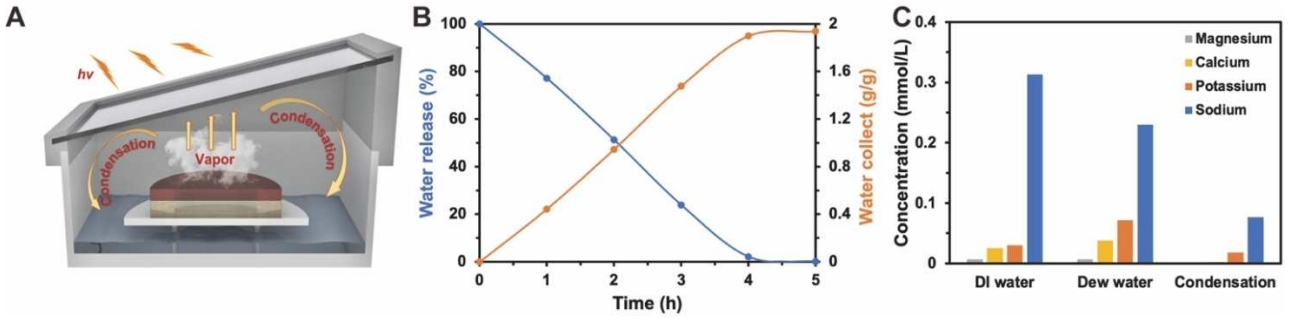

Figure 7. A) Self-designed AWH equipment for water releasing experiment. B) Practical test of atmospheric water adsorption and sunlight-assisted water releasing of AWH hydrogel. C) ICP-MS of DI water, dew water, and the condensed water from the dual-layered hydrogel for ions concentration measurement.

cover. Both container and rectangular cap are made of polystyrene. The inner shell of the container is covered by aluminum foil for enhanced heat accumulation during water desorption. The sloping top cover of the container is made from polyvinylidene chloride (PVC) film (cling wrap) for strong light transmission, while the hydrophobic PVC film is also great for water droplets movement. An enlarged DLH was prepared for the practical test. The water adsorption experiment was conducted during February 2022 at Sydney suburb, Australia, where the average temperature before sunrise was 19 °C, wind speed was 4 km h^{-1}, atmospheric pressure was 102.5 kPa, and relative humidity was ca. 80% R.H (the dew point was approximate 17.5 °C). After a continuous 8 h of water adsorption, the DLH sample showed an adsorption capacity of 1.94 g g^{-1}, with no sign of layer detachment or structural damage. The water release was then achieved by exploring the device under sunlight for 5 h. We observed that 50% of adsorbed water was released within 2 h with a consistent water releasing rate, and almost 100% of captured water was collected after 4 h irradiation (Figure 7B). We also noted that the water vapor condensed on the inner wall of the PVC film at the top cover of the container and then formed small droplets, which can refract and reflect sunlight, reducing the intensity of sunlight. The use of transparent super-hydrophobic cover may alleviate these effects. ICP-MS was used to measure the quality of the produced water, environmental dew water, and deionized water. As shown in Figure 7C, the concentrations of Na^+ (C_{Na+}) and K^+ (C_{K+}) of the condensed water were 0.077 mmol L^{-1} and 0.018 mmol L^{-1} respectively, which were much lower than the C_{Na+} and C_{K+} of DI water and dew water. This result implies that the liquid water produced by the DLH far exceeds the drinking water quality standards set by the World Health Organization.[48,49]

This DLH hydrogel exhibits outstanding water harvesting performance in both laboratory and practical experiments, suggesting its application potential in a real natural environment. Here, we reasonably provide the following potential application according to the environmental temperature and relative humidity record from Australian government Bureau of Meteorology. In Sydney, Australia, which is dominated by a humid subtropical climate, the average temperature in the early morning from November to April (summer season) is about 25 °C and the relative humidity is 74%. At night, the lowest temperature is between 15–18 °C, which means that night-time air humidity in Sydney can often reach or exceed 90% R.H. Similar climatic environments also appear in Zimbabwe, Zambia, Botswana in Africa, Uruguay in South America, southern Brazil, north-eastern Argentina, Alabama, Georgia, Florida in the south-eastern United States, as well as Fujian Province, Guangdong and other southern-coastal areas in China. In a desert climate with a harsher environment, take the Ayers Rock region in the subtropical desert climate in the Northern Territory of Australia as an example. The average summer temperature in the Ayers Rock region is 35 °C during the daytime (average humidity = 20%), and below 20 °C at night. Despite the elevated temperature during the daytime, the

warmer air has potential containing more water vapor, so that the relative humidity in this area at night can reach more than 80% R.H. The climatic conditions in these regions allow the DLH to perform optimally for efficient atmospheric water harvesting, which is significant for reducing carbon emissions and providing a low-cost, stable supply of drinking water worldwide.

Conclusions

In this study, we reported a promising design strategy, "divide and conquer", to construct composite dual-layered hydrogel (DLH) materials for atmospheric water harvesting (AWH) applications that separated the water adsorption and autonomous sunlight-assisted water releasing via two layers. This strategy minimized the functional inhibition caused by poor interfacial compatibility and maintained stable interlayer connections. The water adsorption layer (WAL) achieved an efficient water adsorption, and the light-to-heat conversion layer (LHL) can heat up the DLH above 50 °C under sunlight, thereby promoting efficient water release. The prepared DLH exhibits excellent water adsorption and release performance under high to moderate humidity conditions. More importantly, the water adsorption performance of this DLH was improved by 60% compared to the conventional hybrid hydrogel counterpart. We thus believe that the new strategy of dual-layered AWH hydrogels represents a promising design for the preparation of next-generation, high performance AWH materials.

Experimental Section

Materials

N,N′-Methylenebis(acrylamide) (MBAm, 99%, Sigma-Aldrich), *N*-isopropylacrylamide (NIPAM, 97%, Sigma-Aldrich), [2-(acryloyloxy)ethyl]trimethylammonium chloride solution (AEtMA, 80 wt% in H_2O, Sigma-Aldrich), *N,N,N′,N′*-tetramethylethylenediamine (TEMED, 99%, Sigma-Aldrich), ammonium persulfate (APS, 98%, Sigma-Aldrich), potassium permanganate ($KMnO_4$, 99%, Sigma-Aldrich), potassium sulphate (K_2SO_4, AR, Ajax Finechem Pty Ltd), dopamine hydrochloride (DA, 98%, Sigma-Aldrich), sodium hydroxide (NaOH, 98%, Sigma-Aldrich), sodium bromide (NaBr, 99%, Sigma-Aldrich), and magnesium chloride ($MgCl_2$, 98%, Sigma-Aldrich) were used as received without further purification. Deionized water (DI water) was obtained by Milli-Q water purification system (18.2 MΩ.cm @25 °C). Dialysis tube (SnakeSkinTM, MWCO = 3500) was purchased from Thermo Scientific.

Characterization

UV-VIS-NIR spectra were recorded on a SHIMADZU UV-1700 UV-Visible spectrophotometer. Fourier-transform infrared spectroscopy (FTIR) spectra was obtained using a SHIMADZU MIRacle 10 single reflection ATR accessory. Scanning electron microscope (SEM) images were obtained by Zeiss EVO LS15 SEM system. Infrared thermometer images were captured using FLUKE PTi120 thermal imager. Sunlight simulation light source was obtained from Beijing NBeT HSX-F300 xenon light source. Dynamic light scattering (DLS) data were recorded using a MALVERN Instruments Zetasizer Nano series system. Inductivity coupled plasma mass spectrometry (ICP-MS) characterization was conducted using an Agilent Technologies 7900 ICP-MS system with SPS-4 Autosampler.

Synthesis of PDA–Mn NPs and PDA–Fe NPs

In a typical synthesis, 0.3064 g dopamine hydrochloride was dissolved in 185 mL DI water. Then, 1 M sodium hydroxide was dropwise added into the dopamine solution until the pH of the mixture reached 9 (solution A). This flask was then transferred to ultrasonication for preparation. Dissolving 0.1054 g potassium permanganate (or 0.0973 g iron(III) chloride) in 15 mL DI water (solution B). Once the ultrasonication started, slowly mixed the as-prepared solution B with solution A. The flask was exposed to air for oxygen supply, and the reaction processed for 6 h under sonication at ambient condition (i.e., 1 atm, 22 °C). To purify the obtained NPs, the reaction mixture was dialyzed against DI water using a dialysis Tube (MWCO = 3500 Da) until the color of DI water was clear and transparent. The resultant NPs was then centrifuged and dried at 60 °C in a drying oven for 24 h.

Preparation of the DLHs

For a typical synthesis of the dual-layered hydrogel (LHL/WAL = 1 : 3 *wt/wt*, where LHL = light-to-heat conversion layer, and WAL = water adsorption layer), 0.0567 g NIPAM, 0.003 g MBAm (crosslinker), and 0.009 g PDA–Mn NPs (photothermal material, PTM) were mixed and dissolved in 1 mL DI water under sonication (solution C). 0.0428 g NIPAM, 0.009 g MBAm (crosslinker), and 128 μL AEtMA (80 wt% in water) were mixed and dissolved in 3 mL DI water under sonication (solution D). Then, 3 and 9 μL TEMED were added into solution C and D, respectively. To start the gelation, 50 μL APS solution (0.53 M) was added into solution C to induce polymerization. After gelation of LHL, 150 μL APS solution (0.53 M) was added into solution D, and the mixture was poured on the surface of LHL immediately. The polymerization of WAL was conducted for 2 h. The as-prepared DLH was soaked in DI water for 3 h to remove unreacted residue and freeze-dried for 12 h before vapor adsorption tests.

Moisture adsorption experiments

The moisture adsorption tests were conducted under 3 L min^{-1} air flow with different relative humidity (R.H.%). Dried compressed air was blown to supersaturated salt solution, then the humidified air flows to the surface of WAL of the hydrogel. The R.H. of the air flow were stabilized using potassium sulphate (R.H. = 95%), potassium chloride (R.H. = 90%), sodium bromide (R.H. = 60%) and magnesium chloride (R.H. = 30%).[50] As shown in Scheme S1A, in a 500 mL flat bottom flask, 25 g potassium sulphate was dissolved in 200 mL DI-water. The pipe that flowed dried compressed air was immersed under the level of the supersaturated potassium sulphate solution. Wet air was blown to a container that held the hydrogel. The relative humidity of the gas flow through the saturated salt solution was recorded by a humidity meter (testo-635). We found that the recorded values are close to the theoretical values. During the water adsorption process, DLH was placed in a cylindrical plastic container with a diameter of 4.5 cm and a height of 5 cm without contacting the bottom and sides of the container (the WAL surface was in contact with the air, while the LHL surface was in contact with the hydrophobic support material).The $^3/_4$ height of the container is placed in an ice-water bath, and humid air is blown from the top of the container and cooled down to 5 °C in the container to simulate the low temperature environment at night. The temperature profile of humid air was provided in Scheme S1B.

To prevent the absorption of condensed liquid water, hydrogel in the container was held on a shelf that prevents the hydrogel contacting with the bottom of the container. The mass of the hydrogel was recorded and the condensed liquid water in the container was removed every 30 min.

Sunlight-assisted autonomous water release

The indoor sunlight simulation experiment was conducted using a XE300WUV Xenon light source (Beijing NBeT Technology Ltd) to simulate sunlight. The irradiation intensity was stabilized at 1 kW m^{-2} (1 sun equivalent). The mass of hydrogel was monitored using an analytical balance with internal calibration (OHAUS Pioneer® analytical balance) every 15 min. The surface temperature of the hydrogel was recorded by IR camera (FLUKE PTi120 thermal imager).

Durability test

The durability of the dual-layered hydrogel was determined at 95% R.H. for 10 cycles (for each cycle, we performed water adsorption for 8 h, followed by 4 h indoor simulated sunlight irradiation). At the end of each cycle, the hydrogel was further irradiated for 1 h to remove any potential water residue. The hydrogel was placed with WAL upward during water adsorption, and LHL upward during sunlight irradiation.

Supplementary Data

Information associated with this article can be found in the Supporting material.

Acknowledgements

Q. F. acknowledges the Australian Research Council under the Future Fellowship (FT180100312). A. F. acknowledges support of the International Research Scholarship from the University of Technology Sydney. Open Access publishing facilitated by University of Technology Sydney, as part of the Wiley - University of Technology Sydney agreement via the Council of Australian University Librarians.

Conflict of Interests

The authors declare no conflicts of interest.

Data Availability Statement

The data that support the findings of this study are available from the corresponding author upon reasonable request.

Keywords: atmospheric water harvesting · dual-layered hydrogel · free radical polymerization · polydopamine-manganese nanoparticle · quaternary ammonium salt monomer

[1] P. H. Gleick, *Pacific Institute for Studies in Dev., Environment & Security. Stockholm Env. Institute, Oxford Univ. Press. 473p* **1993**, *9*, 1051–0761.
[2] X. Zhou, H. Lu, F. Zhao, G. Yu, *ACS Materials Lett.* **2020**, *2*, 671–684.
[3] V. Srinivasan, E. F. Lambin, S. M. Gorelick, B. H. Thompson, S. Rozelle, *Water Resour. Res.* **2012**, *48*, W10516.
[4] Y. Tu, R. Wang, Y. Zhang, J. Wang, *Joule* **2018**, *2*, 1452–1475.
[5] Y. Guo, J. Bae, Z. Fang, P. Li, F. Zhao, G. Yu, *Chem. Rev.* **2020**, *120*, 7642–7707.
[6] A. Entezari, M. Ejeian, R. Wang, *ACS Materials Lett.* **2020**, *2*, 471–477.
[7] A. Entezari, M. Ejeian, R. Wang, *Appl. Therm. Eng.* **2019**, *161*, 114109.
[8] J. Xu, T. Li, J. Chao, S. Wu, T. Yan, W. Li, B. Cao, R. Wang, *Angew. Chem. Int. Ed.* **2020**, *59*, 5202–5210.
[9] G. Yilmaz, F. Meng, W. Lu, J. Abed, C. Peh, M. Gao, E. Sargent, G. Ho, *Sci. Adv.* **2020**, *6*, eabc8605.
[10] F. Zhao, X. Zhou, Y. Liu, Y. Shi, Y. Dai, G. Yu, *Adv. Mater.* **2019**, *31*, 1806446.
[11] B. Chen, X. Zhao, Y. Yang, *ACS Appl. Mater. Interfaces* **2019**, *11*, 15616–15622.
[12] X. Wang, X. Li, G. Liu, J. Li, X. Hu, N. Xu, W. Zhao, B. Zhu, J. Zhu, *Angew. Chem. Int. Ed.* **2019**, *58*, 12054.
[13] R. Li, Y. Shi, M. Wu, S. Hong, P. Wang, *Nano Energy* **2020**, *67*, 104255.
[14] P. K. Marwah, G. Paik, C. J. Issa, C. C. Jemison, M. B. Qureshi, T. M. Hanna, E. Palomino, K. R. Maddipati, D. Njus, *Neurotoxicology* **2022**, *90*, 10–18.
[15] M. Salomäki, T. Ouvinen, L. Marttila, H. Kivelä, J. Leiro, E. Mäkilä, J. Lukkari, *J. Phys. Chem. B* **2019**, *123*, 2513–2524.
[16] M. Wu, R. Li, Y. Shi, M. Altunkaya, S. Aleid, C. Zhang, W. Wang, P. Wang, *Mater. Horiz.* **2021**, *8*, 1518–1527.
[17] B. Bolto, J. Gregory, *Water Res.* **2007**, *41*, 2301–2324.
[18] S. Kawamura, *J. Am. Water Works Assoc.* **1991**, *83*, 88–91.
[19] E. M. Wilts, J. Herzberger, T. E. Long, *Polym. Int.* **2018**, *67*, 799–814.
[20] B. Bolto, *J. Water Supply: Res. T.* **2005**, *54*, 531–544.
[21] G. U. Bhaskar, S. Gupta, *Water Air Soil Pollut.* **1987**, *35*, 251–260.
[22] P. Wei, W. Chen, Q. Song, Y. Wu, Y. Xu, *Cellulose* **2021**, *28*, 3723–3732.
[23] T. Alonso-García, C. A. Gervasi, M. J. Rodríguez-Presa, E. Gutiérrez-Pineda, S. E. Moya, O. Azzaroni, *J. Phys. Chem. C* **2013**, *117*, 26680–26688.
[24] I. Yudovin-Farber, N. Beyth, E. I. Weiss, A. J. Domb, *J. Nanopart. Res.* **2009**, *12*, 591–603.
[25] Y. Hu, Z. Fang, X. Ma, X. Wan, S. Wang, S. Fan, Z. Ye, X. Peng, *Appl. Mater. Today* **2021**, *23*, 101076.
[26] A. Cadiau, J. S. Lee, D. Damasceno Borges, P. Fabry, T. Devic, M. T. Wharmby, C. Martineau, D. Foucher, F. Taulelle, C. H. Jun, *Adv. Mater.* **2015**, *27*, 4775–4780.
[27] Q. Wu, W. Su, Q. Li, Y. Tao, H. Li, *ACS Appl. Mater. Interfaces* **2021**, *13*, 38906–38915.
[28] G. Wißmann, A. Schaate, S. Lilienthal, I. Bremer, A. M. Schneider, P. Behrens, *Microporous Mesoporous Mater.* **2012**, *152*, 64–70.
[29] N. Hanikel, M. S. Prévot, O. M. Yaghi, *Nat. Nanotechnol.* **2020**, *15*, 348–355.
[30] A. J. Rieth, A. M. Wright, G. Skorupskii, J. L. Mancuso, C. H. Hendon, M. Dincă, *J. Am. Chem. Soc.* **2019**, *141*, 13858–13866.
[31] S. M. T. Abtab, D. Alezi, P. M. Bhatt, A. Shkurenko, Y. Belmabkhout, H. Aggarwal, Ł. J. Weseliński, N. Alsadun, U. Samin, M. N. Hedhili, *Chem* **2018**, *4*, 94–105.
[32] H. Maher, T. H. Rupam, K. A. Rocky, R. Bassiouny, B. B. Saha, *Energy* **2022**, *238*, 121741.
[33] V. Bon, I. Senkovska, I. A. Baburin, S. Kaskel, *Cryst. Growth Des.* **2013**, *13*, 1231–1237.
[34] M. F. Chaplin, *Water and Life: The unique properties of H_2O*, CRC Press, **2007**, 69–86.
[35] N. N. Greenwood, A. Earnshaw, *Chemistry of the Elements*, Elsevier, **2012**.
[36] C. Czeslik, J. Jonas, *Chem. Phys. Lett.* **1999**, *302*, 633–638.
[37] T. E. de Oliveira, D. Mukherji, K. Kremer, P. A. Netz, *J. Chem. Phys.* **2017**, *146*, 034904.
[38] R. Li, Y. Shi, M. Alsaedi, M. Wu, L. Shi, P. Wang, *Environ. Sci. Technol.* **2018**, *52*, 11367–11377.
[39] D. K. Nandakumar, Y. Zhang, S. K. Ravi, N. Guo, C. Zhang, S. C. Tan, *Adv. Mater.* **2019**, *31*, 1806730.
[40] A. Kabir, M. J. Dunlop, B. Acharya, R. Bissessur, M. Ahmed, *RSC Adv.* **2018**, *8*, 38100–38107.
[41] F. Ni, N. Qiu, P. Xiao, C. Zhang, Y. Jian, Y. Liang, W. Xie, L. Yan, T. Chen, *Angew. Chem. Int. Ed.* **2020**, *59*, 19237–19246.
[42] A. Karmakar, P. G. Mileo, I. Bok, S. B. Peh, J. Zhang, H. Yuan, G. Maurin, D. Zhao, *Angew. Chem. Int. Ed.* **2020**, *59*, 11003–11009.

[43] F. Fathieh, M. J. Kalmutzki, E. A. Kapustin, P. J. Waller, J. Yang, O. M. Yaghi, *Sci. Adv.* **2018**, *4*, eaat3198.
[44] Y. Tao, Q. Li, Q. Wu, H. Li, *Mater. Horiz.* **2021**, *8*, 1439–1445.
[45] H. Qi, T. Wei, W. Zhao, B. Zhu, G. Liu, P. Wang, Z. Lin, X. Wang, X. Li, X. Zhang, *Adv. Mater.* **2019**, *31*, 1903378.
[46] J. Wang, Y. Dang, A. G. Meguerdichian, S. Dissanayake, T. Kankanam-Kapuge, S. Bamonte, Z. M. Tobin, L. A. Achola, S. L. Suib, *Environ. Sci. Technol. Lett.* **2019**, *7*, 48–53.
[47] X. Liu, W. Wang, S. Xie, Q. Pan, *Sci. Rep.* **2021**, *11*, 1–10.
[48] W. H. Organization, *International standards for drinking-water*, **1963**.
[49] I. M. Sayre, *Amer. Water Works Assoc.* **1988**, *80*, 53–60.
[50] E. A. Müller, F. R. Hung, K. E. Gubbins, *Langmuir* **2000**, *16*, 5418–5424.

Manuscript received: January 29, 2023
Revised manuscript received: April 5, 2023
Accepted manuscript online: April 5, 2023
Version of record online: ■■, ■■

RESEARCH ARTICLE

Through a novel 'divide & conquer' strategy, dual-layered hydrogels composed of a water adsorption layer and a light-to-heat layer are developed for atmospheric water harvesting. The hydrogel system manages to achieve a high-water adsorption capacity of 7.73 $g\,g^{-1}$ and low water retention of $< 2\%$ simultaneously.

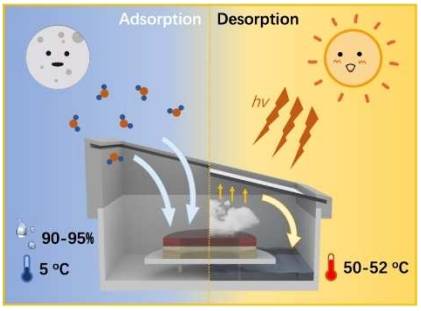

*A. Feng, C. Onggowarsito, S. Mao, Prof. G. G. Qiao, Dr. Q. Fu**